Internal excitation of intermediate mass fragments from collisions of ^{36}Ar + Ag nuclei at 35 MeV/nucleon

F. Deák, Á. Horváth, and Á. Kiss
Department of Atomic Physics, Eötvös Loránd University, H-1088 Puskin u. 5-7, Budapest, Hungary

Z. Seres
KFKI Research Institute for Particle and Nuclear Physics, H-1525 Budapest 114, Hungary

A. Galonsky, C. K. Gelbke, H. Hama,* L. Heilbronn,† D. Krofcheck,‡ W. G. Lynch, D. W. Sackett,§ H. R. Schelin,‖ and M. B. Tsang
National Superconducting Cyclotron Laboratory and Department of Physics and Astronomy, Michigan State University, East Lansing, Michigan 48824

J. Kasagi
Laboratory of Nuclear Science, Tohoku University, Mikamine 1-2-1, Taihaku, Sendai 982, Japan

T. Murakami
Department of Physics, Kyoto University, Kyoto 606-01, Japan
(Received 26 January 1995)

Population ratios for neutron-unbound states compared to bound states were determined for intermediate mass fragments from ^{36}Ar + Ag collisions at 35 MeV/nucleon. The population ratios were measured as a function of fragment kinetic energy at angles of 15°, 30°, 45°, and 60°, especially for ^{12}B fragments but also for ^{7}Li, ^{8}Li, ^{11}Be, and ^{13}C fragments. The results show no major dependence on either the kinetic energy or the emission angle of the fragments. There are signs of a moderate contribution to the dominating statistical decay from nonequilibrium quasielastic decay at the smaller angles. The population ratios for the different fragments are consistent with emission from a source of a single temperature which emits complex nuclei at freeze-out. Comparision of the present results with those from a similar experiment, but with ^{14}N projectiles at 35 MeV/nucleon, shows that the population ratios for strongly damped processes are the same for both ^{14}N and ^{36}Ar projectiles on Ag.

PACS number(s): 25.70.Lm

I. INTRODUCTION

Production of intermediate-mass fragments (IMF's) with $3 \leq Z$ and $6 \leq A$ is one of the prominent features of intermediate energy ($20 \leq E/A \leq 200$ MeV) nucleus-nucleus collisions (see, e.g., [4]). Unlike lighter particles, IMF's are generally excited after leaving a hot nuclear system formed in a heavy-ion reaction. The excitation energy is a source of information different from energy and angular distributions, IMF correlations, and other properties of the emitted particles which are usually investigated [1–5]. Indeed, there is a series of questions connected with the internal excitation of the emitted IMF's which have to be answered by any fragment production model in order to understand the dynamics of nucleus-nucleus collisions.

Thus far it has not been possible to make a straightforward connection between nuclear temperatures derived from the kinetic energy spectra and from the relative populations of the different states of the emitted IMF's [2]. These observables should be related. The slopes of the kinetic energy spectra of the emitted particles determine the temperature of the emitting region [6,7]. At the same time, complementary information about the temperature of the fragmenting system may be obtained from relative populations of ground and excited states of the emitted IMF's, as — according to statistical models — the ratio of populations is determined by the temperature of the emitting system [2,5]. Nuclear temperatures derived from kinetic energy spectra are always much higher than temperatures derived from population ratios of IMF states. For example, with projectiles of ^{14}N at 35 MeV/nucleon, the temperatures from kinetic

*Present address: UVSOR, Institute for Molecular Science, Okazaki, Japan.
†Present address: MS 29-100, Lawrence Berkeley Laboratory, Berkeley, CA 94720.
‡Present address: Lawrence Berkeley Laboratory, Berkeley, CA 94720.
§Present address: NITON Corporation, 74 Loomis Street, Bedford, MA 01730.
‖Present address: Centro Federal de Educacão Technologica, Av. Sete de Setembro 3165 80230-901, Curitiba, Pr, Brazil.

energy spectra were 10–13 MeV but only 2.5–3 MeV from population ratios [1,2]. The discrepancy has not been resolved by taking into account the fact that sequential feeding from higher-lying states may alter the measured populations of the ground and excited states from what they were at freeze-out. Detailed calculations show that the population temperatures are still much lower than the kinetic energy temperatures, and there is no hope of finding basic improvements in the side-feeding model which could account for the discrepancy [2,5].

Multiple IMF emission has been observed in many intermediate-energy, heavy-ion reactions, and it becomes an important reaction channel in the bombarding energy range from about 20 to 60 MeV/nucleon [8,4]. Obviously, the internal excitation of an IMF and the dependence on its kinetic energy may show characteristics of the actual reaction mechanism. Indeed, the various models of single- or multiple-IMF production predict different degrees of internal excitation depending on the kinetic energy of the emitted fragment. For example, in statistical compound nucleus decay the first emitted IMF has the same population ratios no matter what the value of the kinetic energy is. However, in sequential decay more than an IMF which was emitted later in the sequence leaves from a cooler source, and therefore its kinetic energy and internal excitation should both be lower on the average. Generally, sequential decays from an expanding hot nuclear system will lead to different internal excitations as a function of kinetic energy. On the other hand, in a model consisting of an expanding and emitting source, Friedman [9] has shown that though the system proceeds through a sequence of temperatures, there is a characteristic temperature for emission (approximately 5 MeV) which is nearly independent of the incident energy, of the initial temperature, and of the properties of the IMF. In addition, there are other effects which, in principle, also can change the populations of the states after freeze-out. One of them is the possible Coulomb excitation of the IMF as it leaves the electric field of the emitting system. Another possibility is interactions of the IMF with nucleons emitted from other residues [10]. These phenomena could lead to a kinetic energy dependence of the excitation of the IMF, and they have not been investigated in detail.

Unfortunately, there is only limited knowledge about the dependence of the population ratios on the kinetic energy of the IMF [11,12,1,2,5]. Most of the data for population ratios are for a set of events which integrate over IMF kinetic energy [13]. Therefore, the analysis eventually averages over regions with perhaps very different population ratios. IMF's emitted from clearly different reaction mechanisms, like quasielastic or strongly damped processes, have markedly different kinetic energy distributions which may change rapidly with the observation angle [14]. The different mechanisms dominate at different impact parameters and can be attributed to various sections of the kinetic energy spectra.

In earlier works [1,2] it was shown for the ^{14}N + Ag system at 35 MeV/nucleon that the dependence of the neutron-unbound-state–bound-state population ratio on fragment kinetic energy differs for the quasielastic and deep-inelastic data. For a quasielastic IMF whose mass is close to the mass of the beam particles, the ratio decreases towards zero as the fragment velocity approaches the beam velocity. In particular, there was a strong kinetic energy dependence of the relative populations of the first neutron-unbound state and the bound states of ^{12}B. In contrast, the ratio for approximately half-beam mass quasielastic fragments seems to be constant or only slightly decreasing with increasing kinetic energy. On the other hand, the ratio for deep-inelastic IMF's is approximately independent of kinetic energy and perhaps even independent of fragment mass.

The results of former experiments leave most of the problems open and raise new questions. Are these observations about the internal excitation of the emitted IMF's generally true for intermediate energy heavy-ion reactions? Do the population ratios support the assumption of a single IMF production mechanism and source in the intermediate energy heavy-ion processes? How does the emitting source evolve in space and time in the nucleus-nucleus collision process and from which temporal phase are the IMF's emitted? Is there any dependence of the internal excitation of the IMF's on the internal structure and identity of the emitted fragments? What are the angle and energy distributions of the excited fragments? Dependence on emission angle can be expected for emission from nonequilibrium nuclear systems. Is there any dependence of the internal excitation of the IMF on detection angle? Do the population ratios of the states of IMF's reflect the various reaction mechanisms thought to dominate the different kinetic energy regions? In particular, we proposed a stripping–pick-up model for quasielastic IMF production which explained the data well for reactions induced by ^{14}N at 35 MeV/nucleon on several targets from the light to the heavy nuclei [15,7,16]. The same model gave a plausible explanation of the kinetic energy dependence of the internal excitation for quasielastic IMF's. How does the model perform for IMF's with mass far away from the mass of the projectile?

In order to have a general insight into the dependence of IMF internal excitation on IMF velocity, we concentrated on the IMF ^{12}B, which was found earlier [1] to have advantageous properties for this purpose. In particular, the cross sections for ^{12}B nuclei emitted in their 3.388-MeV, first neutron-unbound state and in their particle stable states should be determined. The latter can be obtained from ^{12}B singles measurements, and the former from ^{11}B – neutron coincidences. The measured cross-section ratios of these states can be used to calculate temperatures from a Boltzmann population distribution. The population ratio (R) of two states of the same nucleus is related to the population temperature (T) in the following way:

$$R = \frac{2J_1 + 1}{2J_2 + 1} \exp(-\Delta E/T), \tag{1}$$

where J_1 and J_2 are the spins of the two states, and ΔE is the energy difference between them.

Since the neutron decay energy of the narrow 3.388-MeV state is only 18 keV (Γ is only 3.1 eV), most of

the emitted neutrons will be kinematically focused into detectors positioned collinear to the target-fragment detector. The feasibility of collinear geometry is a direct consequence of using neutrons, which are not sensitive to some additional distorting effects of the Coulomb field of the emitting fragments and can penetrate a fragment detector. As ^{12}B is generally produced with considerable cross sections in heavy-ion collisions at intermediate energies [17], this method provides an excellent "thermometer" for the measurement of the internal temperature as a function of the kinetic energy of the IM fragments. Methods using charged particles [5] differ in effectiveness and give complementary results.

The purpose of this paper is to present experimental data on the kinetic energy and angle dependence of the internal excitation of IMF's emitted from the ^{36}Ar + Ag system at 35 MeV/nucleon by measuring IMF singles and IMF-neutron coincidences in collinear geometry. The ^{36}Ar beam was chosen in order to have some IMF's, especially the ^{12}B, with mass far from the mass of the bombarding particles. However, the incident ^{36}Ar, as the earlier used ^{14}N nucleus, has an equal number of neutrons and protons. The target and the beam energy were the same as in a previous investigation [2]. The experiment was optimized for the ^{12}B thermometer, but as in the earlier study [2] other IMF's, especially Li, Be, and C isotopes, where excitation of neutron-unbound states could be observed, were evaluated as well.

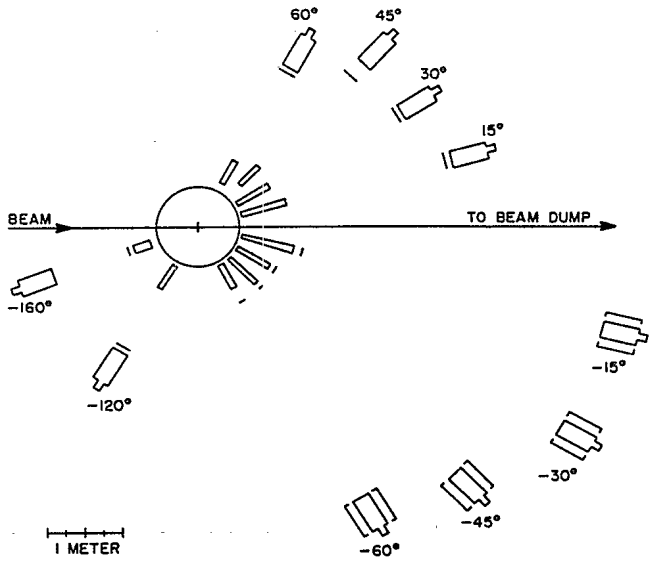

FIG. 1. Outline of the experimental setup. The symbols with angle labels represent neutron detectors or close-packed bundles of three detectors (-15°) or of seven detectors (-30°, -45°, -60°, -120°). The rectangular boxes represent shadow bars which were in place about half of the time, and the solid lines behind the shadow bars represent proton veto paddles. The circle represents the scattering chamber in which the collinear IMF telescopes (not shown) were placed.

II. EXPERIMENTAL PROCEDURE

The experiment was performed at the K500 cyclotron of the National Superconducting Cyclotron Laboratory of Michigan State University. Most of the apparatus and techniques used were similar to those used in earlier investigations [18,16,2]. Some results on neutron and fragment isotope inclusive spectra which were determined from the present set of experimental data were published earlier [19,17,20].

The incident beam was $^{36}Ar^{11+}$ at 35 MeV/nucleon with 10^9 ions/sec intensity. Natural silver targets of 2.2 mg/cm^2 and 2.57 mg/cm^2 areal densities were used in some runs perpendicular and in others at 60° to the beam. The outline of the experimental setup, without the fragment detection systems, is shown in Fig. 1.

The IMF's were detected with $\Delta E - E$ silicon detector telescopes [17]. They were placed inside the scattering chamber of 1 m diameter at angles of 15°, 30°, 45°, 60°, and 120° in the horizontal plane on the right side of the beam (in Fig. 1 below the beam line) and one at 45° out of this plane directly below the beam axis. The telescopes consisted of 2 to 4 elements, the number depending on the detection angle. The first ΔE detectors were 30 μm in thickness, allowing isotopic separation (see later) from $Z = 4 - 10$ down to $E/A = 2 - 10$ MeV — 2 MeV for the lighter fragments and 10 MeV for $Z = 10$. The second ΔE detectors were 100 μm thick. The E detectors stopped all IMF's up to at least 40 MeV/nucleon. Every element was cooled to $-10\,^{\circ}$C. The solid angles of the Si telescopes were about 10 msr. In order to reduce the number of small pulses from electrons and x rays produced in the target, a gold foil of $\sim$ 10 mg/cm^2 was placed in front of each telescope. The telescopes were energy calibrated with the aid of a precision pulse generator. Corrections were made event-by-event for energy loss in the gold foil and the target. The uncertainty in IMF kinetic energy was estimated to be typically 2%. Detector pulses from numerous hydrogen and helium nuclei were rejected with hardware electronics. Separate runs were made intermittently during the experiments to measure fragment singles in order to determine bound-state populations.

The neutron detectors consisted of liquid scintillator (NE-213 or BC-501) in sealed glass cells. Most of the cells had dimensions of about 12.7-cm diameter and 7.6-cm thickness [2]. The intrinsic timing resolution of the neutron detectors, when measured using γ rays from a ^{60}Co source, was 0.9 ns on the average. Closed-packed arrays of neutron detectors were placed in collinear positions with IMF telescopes at 15°, 30°, 45°, and 60° on the right side of the beam at distances ranging from 450 cm (at 15°) to 350 cm (at 60°). The array at 15° consisted of three, while the other three arrays were made of seven neutron detectors. The solid angles of the neutron arrays and those of the corresponding fragment telescopes were optimally matched to each other. Other neutron detectors shown in Fig. 1 were placed at distances from 160 to 250 cm and the data for them were discussed elsewhere [19,20].

In front of each detector array a 6-mm-thick NE102A paddle was placed for the rejection of high energy protons. (Protons which were emitted with energies smaller

than about 40 MeV were stopped by the material between the target and the neutron detector.) Neutrons were distinguished from gamma rays by pulse-shape discrimination using two QDC's [21].

Neutron energies were determined by the time-of-flight technique that used neutron and fragment signals as the start and stop, respectively. The timing signal on the fragment side came from the 100 μm ΔE element of each telescope, and from the anode pulse on the neutron side. The overall timing resolution was determined by evaluating the prompt γ rays in the time-of-flight spectra and it was between 1 and 1.2 nsec for all cases. The energy dependent efficiency of the neutron detectors was computed by a Monte Carlo code [22], and the uncertainty in the efficiencies was estimated to be 10% [15,2]. The attenuation of the neutrons by the material between the target and the neutron detector was taken into account [15,23]. Inscattering background contributions to the neutron spectra were determined by taking data with shadow bars between the target and the neutron detectors (see Fig. 1) during approximately half of the run time.

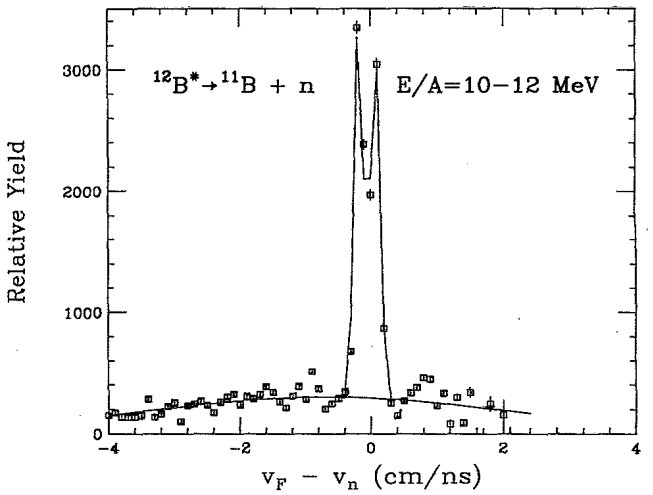

FIG. 2. Typical $V_F - V_n$ relative velocity spectrum for $^{11}B + n$ coincidences at 15° for ^{11}B fragments in a 10 – 12 MeV/nucleon energy bin. The solid line represents the normalized result of a Monte Carlo simulation added to a broad Gaussian background.

III. DATA ANALYSIS

The data were taken in event mode and the analysis was done off line.

The data for the fragment telescope were evaluated using a standard technique for the fragment singles [17]. In every telescope there was good element separation, and the isotope separation was performed by the usual $\Delta E - E$ technique. For each element a two-dimensional energy/nucleon–particle identification spectrum was constructed. These spectra were sliced into energy/nucleon channels, then fitted with Gaussians of a single width for each isotope having significant intensity plus a linear background.

The IMF-neutron collinear cases were handled as described in Refs. [18,2]. First, the identification of the IMF element — Li, Be, B, or C — was performed and the fragment kinetic energy was deduced for each event. Then the neutron velocity was determined and an individual weight factor was calculated which took the efficiency and all the necessary corrections into account event by event. With these data, two-dimensional spectra of $V_F - V_n = \Delta V$ (IMF-neutron relative velocity) versus IMF particle identification value were created for all those events in which the kinetic energy of coincident fragment was in a prescribed bin. In this procedure, the literature value of the mass of the isotope for which we actually wanted to establish the relative velocity spectrum was used in each case [24–26]. The background and shadow bar runs were taken into account as described in Refs. [18,1,2]. These two-dimensional spectra were then cut into ΔV bins of width 1 mm/ns. Finally, each resulting one-dimensional spectrum was fitted with as many Gaussians (of a single width) as there were isotopes of a significant intensity plus a linear background. The area for a given isotope became a point in a relative velocity spectrum for the prescribed fragment kinetic energy bin. As a typical example, Fig. 2 shows the ^{11}B-neutron relative velocity spectrum for ^{11}B in the 10 – 12 MeV/nucleon kinetic energy range at 15°. The small decay energy (19 keV) explains the strong kinematic focusing effect around zero relative velocity.

The populations of the different neutron-unbound states were extracted from the relative velocity spectra by applying the results of Monte Carlo calculations to the experimental data. The code MONTRES [18] simulates the decay of neutron-unbound states into the detection system. All experimental details which influence the detection of fragments or neutrons (target thickness, silicon detector resolution, neutron detector thickness, intrinsic time resolution, solid angles, etc.) were explicitly taken into account. The neutron decay was assumed to be isotropic in the rest frame of the emitting IMF's. The relative velocity spectra were in all cases simulated well by the results of these calculations added onto a broad Gaussian background. As an example, the solid line in Fig. 2 represents the result of the normalized Monte Carlo simulation. Values extracted from the comparisons of the experimental spectra with the calculated ones were directly used for the determination of the production cross sections of the neutron-unbound states [18,2].

IV. EXPERIMENTAL RESULTS

There were 34 isotopes of the IMF elements Li, Be, B, C, N, O, F, Ne, Na, and Mg that could be identified in the singles data taken by the fragment telescopes [17]. Relative velocity spectra were created for all possible cases of IMF-neutron collinear coincidences. Besides the ^{11}B + neutron spectra, for which the experiment was optimized, there were several other isotopes for which the relative velocity spectra could be evaluated. These additional cases were the $^{6}Li + n$, $^{7}Li + n$, $^{10}Be + n$, and

the $^{12}C + n$ coincidences at 15°, 30°, 45°, and 60°.

In the fragment telescope at 120° some Li isotopes and very few Be nuclei were detected in the singles experiment. No event was observed for elements heavier than beryllium, and no IMF-neutron coincidences could be detected for any IMF.

A. Experimental results for the ^{11}B + neutron coincidences

The 18 keV neutron decay of the 3.388-MeV ($J^\pi = 3^-$, $\Gamma = 3.1 \pm 0.6$ eV [25]) state in ^{12}B to the ground state of ^{11}B was observed in collinear geometry from 15° to 60°. Fragment-neutron relative velocity spectra were created in 2 MeV/nucleon wide fragment kinetic energy bins. The lowest evaluated energy bin at each angle was the one in which both the fragments and the neutrons in coincidence with each other were safely over their energy thresholds.

In order to calculate the population ratios, the cross sections for the ground state and the 3.388-MeV neutron-unbound state had to be determined. The ^{12}B spectra were derived from the fragment singles experiment, and they are displayed in Fig. 3 on the right-hand side. The left-hand side shows the spectra for production of the first neutron-unbound state. At each angle the shapes of the two energy spectra are similar.

Figure 4 shows the ratios of the cross sections for the first neutron-unbound state to those for the particle-bound states of ^{12}B as a function of the IMF kinetic energy for the four observation angles. The error bars in Fig. 4 correspond to the statistical uncertainties only. The possible deviations in absolute values of the population ratios are estimated to be about 15%, mainly due to the uncertainties in neutron detection efficiency.

The population ratios obtained at 15° are almost constant over the wide range of fragment kinetic energy from 6 to 42 MeV/nucleon. However, there is a slight decrease toward higher energies. The ratios around the beam velocity are 0.11 ± 0.01, i.e., ~25% lower than the values at low energies (0.14 ± 0.01). It is worth nothing that even at fragment velocities which are higher than the velocity of the incident ^{36}Ar ion, the internal excitation of the ^{12}B fragments does not go to zero and the cross section ratios are close to those at neighboring energies. No systematic trend can be observed in the population ratios at 30° and 45°; both sets of data are consistent with constant internal excitation of ^{12}B. The four data points for 60° measurement covering the fragment kinetic energy range from 4 to 12 MeV/nucleon show perhaps a slight increase of the population ratios with energy. There seems to be a slight increase of the ratio with angle. Also, the trend

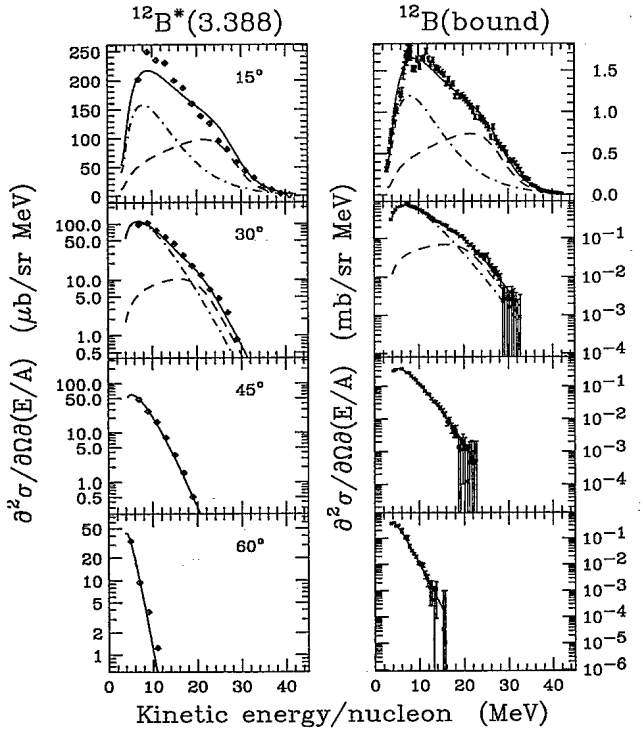

FIG. 3. Energy spectra of ^{12}B (right side) as determined in fragment singles measurements and for ^{12}B in its 3.388-MeV first neutron-unbound state (left side) as determined from the analysis of relative velocity spectra. The solid lines are fits to the cross sections according to the method used in Ref. [14]. For the data at 15° and 30° the decomposition into quasielastic (dashed line) and strongly damped (dot-dashed line) contributions is also shown.

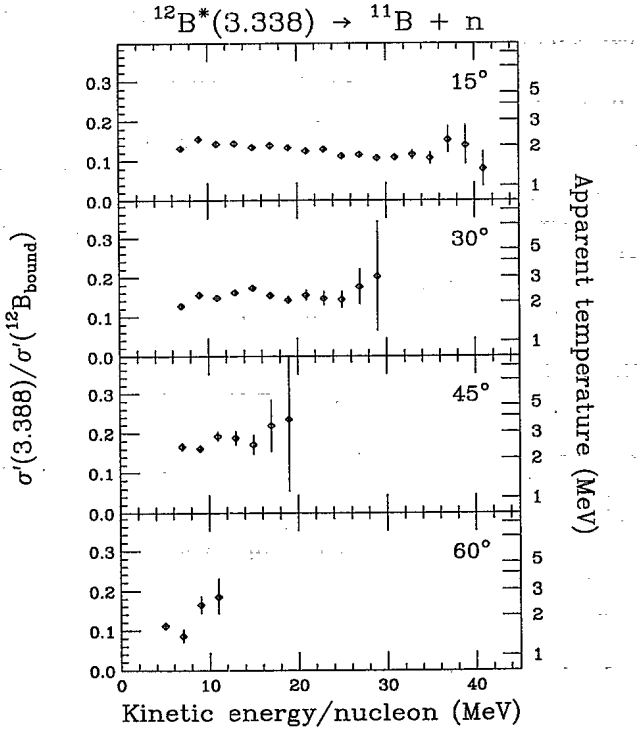

FIG. 4. Ratios of the double differential cross sections for the first neutron-unbound state [$\sigma'(3.388)$] and for the sum of the particle-bound states [$\sigma'(^{12}B_{bound})$] of ^{12}B as a function of the fragment kinetic energy. The error bars correspond to the statistical uncertainties only. On the right side the apparent nuclear temperatures are shown as derived according to Eq. (1).

with kinetic energy/nucleon goes from decreasing to constant to increasing as the angle changes from 15° to 60°.

On the right side of Fig. 4 the values of the apparent nuclear temperature T are shown as derived by using Eq. (1) adapted for more than one bound state. In calculating T, it was assumed that the populations of the four particle-bound excited states of ^{12}B are measured in the ground state channel. The nuclear temperatures which correspond to the measured population ratios range from about 1.5 MeV to 2 MeV at 15° to 2.0 MeV at 30° and about 2.5 MeV at 45°.

B. Experimental results for the Li, Be, and C isotopes

In the ^{6}Li + neutron case we observed the neutron decay of the 7.460-MeV ($J^\pi = 5/2^-$, $\Gamma = 89 \pm 7$ keV [24]) state to the ground state of ^{6}Li. The decay energy is 210 keV. The branching ratio of the ^{7}Li state to decay into the neutron channel is determined by $\Gamma_n/\Gamma_{tot} = 0.776$ [24].

For statistical reasons the width of the fragment kinetic energy bins was increased to 5 MeV/nucleon. The ΔV spectra showed the double peak at ± 8 mm/ns, quite similar to that displayed in Fig. 4 of Ref. [18]. The lowest IMF kinetic energy bin which could be evaluated was that from 5 to 10 MeV/nucleon.

There were two problems in the evaluation of this case which needed further consideration. As the neutron decay energy of the 7.460-MeV state in ^{7}Li and its width are comparable, the energy dependence of the width had to be taken into account in the evaluation of the ΔV spectra. To this aim the method described in Ref. [2] was used in the Monte Carlo simulation of the events. The other problem is connected with the fact that the singles spectra of ^{7}Li contain events from the decay into two α particles of ^{8}Be. When both α particles are detected in the same telescope, the ΔE signal is not distinguishable from a signal produced by a ^{7}Li [27]. In order to make the corrections, the yield of ^{8}Be from strongly damped processes was estimated by using the interpolated value in Fig. 5 of Ref. [17]. For the determination of the quasielastic contribution, a linear interpolation was made between the quasielastic yields of ^{7}Be and ^{9}Be. Assuming the same energy and angular distributions as the neighboring ^{9}Be, a Monte Carlo simulation of the detection of both α particles determined the correction to the measured ^{7}Li spectra.

The left side of Fig. 5 displays the results for the population ratios of the 7.460-MeV and the ground state of ^{7}Li. At 15° the ratio has a slight trend to decrease toward higher energies. The ratio at the four lowest energies scatters around a value of 0.029 ± 0.002 and decreases at higher energies to 0.015 ± 0.004 in the 35 – 40 MeV/nucleon bin. For the larger angles the ratio is consistent with a constant value at each angle, and the value is definitely higher than at 15°. The average of the population ratio for 30° is 0.047 ± 0.003 and for 45° *0.058* ± 0.007. Unfortunately, an underestimate in the quasielastic part of the ^{8}Be correction could lead just to

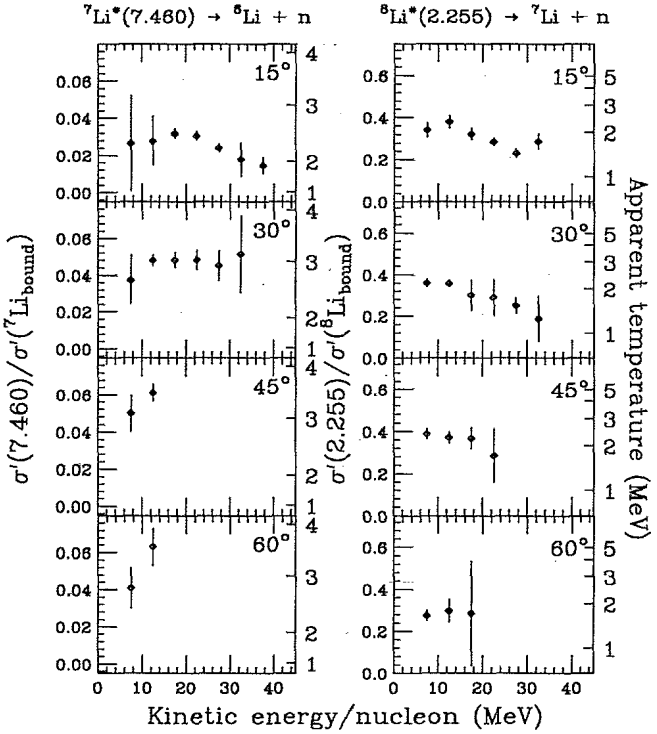

FIG. 5. The population ratios as in Fig. 4, but for the 7.460-MeV state and the bound states of ^{7}Li (left side) and for the 2.255-MeV state and the bound states of ^{8}Li (right side). The fragment kinetic energy bins are 5 MeV/nucleon wide.

similar trends both in kinetic energy dependence at 15° and in angular dependence. The right axis of the left panel of Fig. 5 shows the apparent nuclear temperatures derived by using Eq. (1). It is between 2 and 2.5 MeV for the 15° position, and it is ≥ 3 MeV for the other angles.

The ^{7}Li + neutron relative velocity spectra show prominent peaks at about ± 7 mm/nsec. They correspond to the neutron decay of the 2.255-MeV ($J^\pi = 3^+$, $\Gamma = 33 \pm 6$ keV [24]) state to the ground state of ^{7}Li. The decay energy is 222 keV. The right side of Fig. 5 displays the corresponding population ratios with fragment kinetic energy bins of 5 MeV/nucleon. The ratios at 15° decrease with fragment kinetic energy. This is also seen in the 30° data. The ratios at 45° and the 60° are consistent with constant values. The right axis of the left panel shows the apparent nuclear temperatures for ^{8}Li.

As for the Be isotopes, only the neutrons in coincidence with ^{10}Be have intensities for which an evaluation was feasible. The investigated transition was the 19 keV neutron decay from the 3.887 ± 15 keV ($J^\pi \geq 7/2$, Γ<10 keV) state into the 3.3680-MeV ($J^\pi = 2^+$) first excited state of ^{10}Be [24,25]. The population ratios were derived in 5 MeV/nucleon fragment kinetic energy bins; except the first energy bin ranged only from 7 to 10 MeV/nucleon. In contrast to the other decays, the main uncertainty in this case was provided by the fact that the ^{11}Be isotope could hardly be resolved in the singles spectra in the neighborhood of the relatively intensely populated ^{10}Be. Figure 6 displays the results for ^{11}Be.

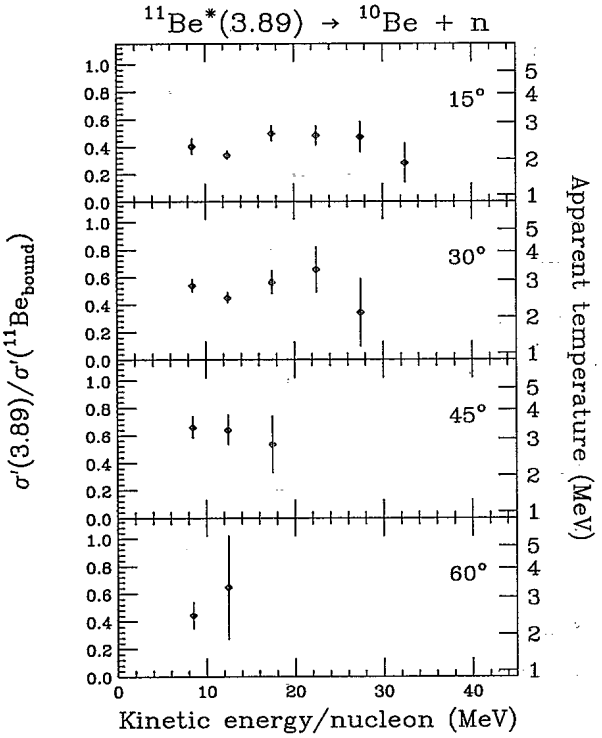

FIG. 6. The population ratios as in Fig. 4 for the 3.890-MeV state and the bound states of ^{11}Be. The fragment kinetic energy bins are 5 MeV/nucleon wide; the lowest bin is 7 – 10 MeV/nucleon.

The ratios do not show any systematic dependence on fragment kinetic energy for any of the angles. However, the average ratio for the 15° position (0.42 ± 0.07) tends to be slightly lower than for 30° (0.51 ±0.08) and 45° (0.61 ±0.1). The average apparent nuclear temperature is about 2.5 MeV for the 15° case and scatters around 3 MeV for the other observation angles.

In the ^{12}C + neutron case the 114 keV neutron decay of the 9.50-MeV ($J^\pi = 9/2^+$, $\Gamma < 5$ keV) state of ^{13}C to the first 4.439-MeV 2^+ excited state of ^{12}C [25,26] was investigated. The decay produced a double peak in the

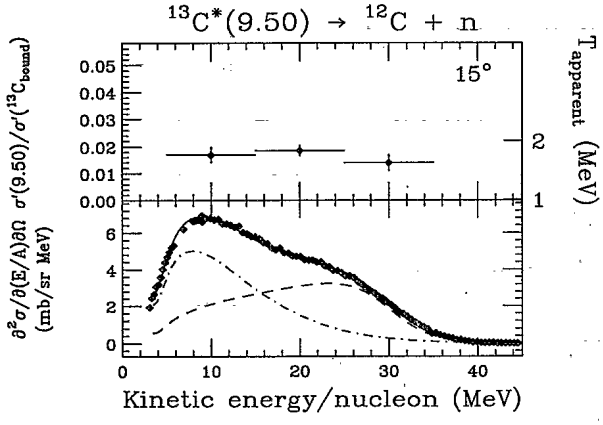

FIG. 7. The population ratios for the 9.50-MeV state and the bound states of ^{13}C at 15° (upper part) and the cross section for the bound states of the same isotope at 15° (lower part). The meanings of the lines are the same as in Fig. 3.

relative velocity spectra at about ± 5 mm/nsec. The ΔV spectra were similar to those shown in Fig. 7 of Ref. [18]. The dependence of the population ratio for the ^{13}C states at 15° is shown in Fig. 7; the lower part of the figure displays the cross sections of the ^{13}C ground state at the same angle. The spectra for the other positions could not be evaluated reliably. The ratios are consistent with a constant for the three different IMF kinetic energies for 15°, corresponding to an apparent nuclear temperature of about 1.8 MeV.

V. DISCUSSION OF THE RESULTS

The most prominent general result of the present study is that there is little dependence of population ratio on either fragment kinetic energy or the observation angle of ^{12}B fragments. Sequential feeding does not depend on the kinetic energy of the parent nucleus. Therefore, from the fact that all the observed ^{12}B fragments have approximately the same population ratio, we may conclude that the internal excitation of the originally emitted fragments was independent of the fragment kinetic energy at the freeze-out as well.

The ^{12}B data do not require a model in which the population ratios are increasing with kinetic energy at any angle. This is in contradiction to models of sequential fragment emission from expanding hot nuclear systems produced in heavy-ion collisions.

The present results markedly deviate from the observations for quasielastic collisions in the ^{14}N + Ag system at 35 MeV/nucleon [1,2]. In those experiments, at 15° a strong fragment kinetic energy dependence was observed: the population ratios were near zero for fragment velocities close to the velocity of the incident beam. The shapes of the ^{12}B spectra at 15° (Fig. 3) show clear signs of the presence of quasielastic events. According to the decomposition of the spectrum into quasielastic and strongly damped parts (dashed and dot-dashed curves in Fig. 3), above ~18 MeV/nucleon the quasielastic process dominates. Yet, at 15° only a moderate (less than 40%) decrease in the population ratios can be seen (Fig. 4) from low kinetic energies up to 35 MeV/nucleon. Even ^{12}B's with velocities larger than the beam velocity have considerable values for the population ratio, and therefore they are on the average hardly less excited than fragments with much lower kinetic energies.

The quasielastic component results from peripheral collisions [18,14,7]. In the stripping–pick-up model, the quasielastic spectra result from a projectile fragmentation into a part that penetrates the target and forms a hot participant zone and a projectilelike spectator part that later picks up material from the expanding hot zone, thus forming a projectilelike fragment. The stripping–pick-up process, which was quite successful in explaining several properties of ^{14}N induced reactions [15,1,7], may not be a major reaction mechanism at ^{12}B kinetic energies around the beam velocity for the ^{36}Ar + Ag system. Instead, a thermal source may be able to emit ^{12}B's with high velocities.

According to the former considerations, the decrease in

population ratios with kinetic energy at 15° is explained by the coexistence of different reaction mechanisms. If one of the mechanisms is that of the stripping–pick-up process, its share can be estimated from the population ratio at the beam velocity. At this velocity the model predicts zero internal excitation for the IMF. Therefore, its share should be less than 40%. A check on these conclusions would be the study of the population ratios beyond the beam velocity. These populations are not influenced by contaminations from cold fragments and should be similar to those at low energies. Unfortunately, the three experimental points above 35 MeV/nucleon have poor statistics (Fig. 4).

The former ideas can qualitatively explain the observed slight angular dependence of the population ratios as well. It can be seen in Fig. 3 that even the 30° fragment spectra may contain contributions from quasielastic processes. As the fragments from this mechanism are cooler than those from statistical decay of a hot source, they can provide for the slightly lower average internal excitation relative to the values at 45° where the spectra are free from quasielastic contamination.

The results for the neutron decay of the excited states of ^{7}Li, ^{8}Li, ^{10}Be, and ^{13}C are consistent with data for ^{12}B. The observations show features which can be explained qualitatively with similar considerations. For the emission of the IMF's, there is a dominant process which produces fragments with about the same internal excitation. In addition to this mechanism, there are minor contributions from nonequilibrium processes.

Dealing with the dominating mechanism, it is interesting to investigate whether the source for the emission of different IMF's could have a single temperature. In order to investigate this question, the average of the population ratios at 45° (where the quasielastic contribution is negligible) for each isotope was compared with the prediction of the sequential feeding model (e.g., [11,28]). We did not perform new calculations as we had the same isotopes, except for ^{11}Be, which were already discussed in Ref. [2]. The only difference between the two systems, ^{14}N+Ag and ^{36}Ar+Ag, is that we now have about 15% more nucleons in the initial nuclear assembly. This may produce a small and perhaps smoothly changing variance of the freeze-out fragment distribution for the same initial temperature. However, as we do not look at the production cross sections but at the ratios of the populations, practically the same results are expected in the case of the same initial temperature. Table I compares the measured and calculated values for 2.5 MeV nuclear temperature. These values are convincingly close to each other. This is consistent with the assumption that there exists an equilibrated source and the dominating mechanism is statistical IMF emission from the same source with one common nuclear temperature for all fragments. This source has, however, a much lower nuclear temperature than the 5 MeV suggested by Ref. [9].

Comparing the population ratios at 45° with those for the strongly damped processes with the ^{14}N beam, they are surprisingly close to each other. Though the values for ^{36}Ar seem to be a bit higher, the deviations are inside the quoted uncertainties. One may wonder how it is possible that nuclear systems which were created in collisions of silver nuclei with a projectile of such different incident energies (490 MeV in the ^{14}N case vs 1260 MeV for ^{36}Ar) emit IMF's with internal excitation so close to each other. An explanation could be that the source of the IMF's is created in interactions of the incoming nucleons with approximately the same number of target nucleons (like the half-beam-velocity intermediate rapidity source [18,7]). In this picture, the thermal properties of the source are determined by the velocity of the incident projectiles, while its size is governed mainly by the number of nucleons in the projectile. Therefore, the multiplicity of the emitted IMF's from this strongly damped source should be greater for the heavier projectile. Rough evidence in favor of such behavior can be seen, e.g., by comparing the cross sections in Fig. 3 with cross sections for ^{11}B in Fig. 1 of Ref. [2]. There evidence is present for all the isotopes common to both experiments. All these results are consistent with the observations for lighter fragments (such as ^{6}Li and ^{7}Li) in the ^{14}N experiments that their internal excitation — though they decrease with the fragment kinetic energy — does not converge to zero around the beam velocity.

TABLE I. Population ratio averaged over kinetic energy for fragments and neutrons emitted at 45°. The ratio is for a neutron-unbound state (excitation energy in MeV in parentheses) to the sum of all bound states. The calculated values are from the sequential feeding calculation of Ref. [2] with 2.5 MeV initial temperature.

Decaying isotope	Calculated ratio	Measured ratio
^{7}Li (7.46)	0.05	0.055± 0.01
^{8}Li (2.255)	0.38	0.38 ± 0.01
^{12}B (3.388)	0.17	0.18 ± 0.01
^{13}C (9.50)	0.03	0.017± 0.02 [a]

[a]This experimental value is for 15°.

There is no explanation for the low value of the apparent nuclear temperature (~2.5 MeV) derived from the study of the population ratios in comparison with those from the kinetic energy spectra. This work proves that the explanation for the low population ratios may not be found in averaging a rapidly changing function of the fragment kinetic energy. Instead, the discrepancy is a sign that the thermal equilibration processes are incomplete for the internal degrees of freedom at the moment of fragment emission.

VI. CONCLUSIONS

The population ratios of several intermediate mass fragments, especially those of ^{12}B, do not show a major dependence on either fragment kinetic energy or observation angle. A comparison with the sequential feeding model makes it probable that there is a source with a single temperature from which the majority of the IMF's are emitted by statistical processes. The slight decrease for fragments in the forward direction of the population ratios with fragment kinetic energy and the rather small angular dependence of these ratios can be considered as a

sign of contamination from preequilibrium fragment formation. There are no major differences in the internal excitations of IMF's from strongly damped processes for the same energy/nucleon ^{14}N and ^{36}Ar beams. This is an indication of the possibility that the IMF's are emitted from a local source without the inclusion of all nucleons of the colliding nuclei [29,3].

ACKNOWLEDGMENTS

The authors wish to thank the cyclotron crew at the NSCL for providing a good beam. This work was supported in part by NSF Grants No. PHY92-14992 and No. INT91-13997, by the Hungarian Academy of Science, and by the CNPq-Brazil.

[1] F. Deák, A. Kiss, Z. Seres, A. Galonsky, C.K. Gelbke, L. Heilbronn, W. Lynch, T. Murakami, H. Schelin, M.B. Tsang, B.A. Remington, and J. Kasagi, Phys. Rev. C **39**, 733 (1989).

[2] L. Heilbronn, A. Galonsky, C. K. Gelbke, W. G. Lynch, T. Murakami, D. Sackett, H. Schelin, M.B. Tsang, F. Deák, A. Kiss, Z. Seres, J. Kasagi, and B.A. Remington, Phys. Rev. C **43**, 2318 (1991).

[3] G.J. Kunde, J. Pochadzalla, J. Aichelin, E. Berdermann, B. Berthier, C. Cerruti, C.K. Gelbke, J. Hubele, P. Kreutz, S. Leray, R. Lucas, U. Lynen, U. Milkau, W.F.J. Müller, C. Ngô, C.H. Pinkenburg, G. Raciti, H. Sann, and W. Trautmann, Phys. Lett. B **272**, 202 (1991).

[4] L.G. Moretto and G.J. Wozniak, Annu. Rev. Nucl. Part. Sci. **43**, 379 (1993).

[5] T.K. Nayak, T. Murakami, W.G. Lynch, K. Schwarz, D. J. Fields, C.K. Gelbke, Y.D. Kim, J. Pochodzalla, M.B. Tsang, H.M. Xu, F. Zhu, and K. Kwiatkowski, Phys. Rev. C **45**, 132 (1992).

[6] B.V. Jacak, G.D. Westfall, G.M. Crawley, D. Fox, C. K. Gelbke, L.H. Harwood, B.E. Hassekquist, W.G. Lynch, D.K. Scott, H. Stöcker, M.B. Tsang, G. Buchwald, and T.J.M. Symons, Phys. Rev. C **35**, 1751 (1987).

[7] F. Deák, Á. Kiss, Z. Seres, A. Galonsky, L. Heilbronn, and H.R. Schelin, Phys. Rev. C **42**, 1029 (1990).

[8] K. Hagel, M. Gonin, R. Wada, J.B. Natowitz, B.H. Sa, Y. Lou, M. Gui, D. Utley, G. Nebbia, D. Fabris, G. Prete, J. Ruiz, D. Drain, B. Chambon, B. Cheynis, D. Guinet, X.C. Hu, A. Demeyer, C. Pastor, A. Giorni, A. Lleres, P. Stassi, J.B. Viano, and P. Gonthier, Phys. Rev. Lett. **68**, 2141 (1992).

[9] W.A. Friedman, Phys. Rev. Lett. **60**, 2125 (1988).

[10] D.H. Boal, Phys. Rev. C **30**, 749 (1984).

[11] J. Pochodzalla, W.A. Friedman, C.K. Gelbke, W.G. Lynch, M. Maier, D. Ardouin, H. Delagrange, H. Double, C. Grégoire, A. Kyanowsky, W. Mittig, A. Péghaire, J. Péter, F. Saint-Laurent, Y.P. Viyogi, B. Zwieglinski, G. Bizard, F. Lefébres, B. Tamain, and J. Québert, Phys. Rev. Lett. **55**, 177 (1985).

[12] C.B. Chitwood, C.K. Gelbke, J. Pochodzalla, Z. Chen, D.J. Fields, W.G. Lynch, R. Morse, M.B. Tsang, D.H. Boal, and J.C. Shillcock, Phys. Lett. B **182**, 155 (1986).

[13] Z. Chen, C.K. Gelbke, W.G. Gong, Y.D. Kim, W.G. Lynch, M.R. Maier, J. Pochadzalla, M.B. Tsang, F. Saint-Laurent, D. Ardouin, H. Delagrange, H. Doubre, J. Kasagi, A. Kyanowski, A. Péghaire, J. Péter, E. Rosato, G. Bizard, F. Lefébvres, B. Tamain, J. Québert, and Y.P. Vijogi, Phys. Rev. C **36**, 2297 (1987).

[14] A. Kiss, F. Deák, Z. Seres, G. Caskey, A. Galonsky, B. Remington, and L. Heilbronn, Nucl. Phys. **A499**, 131 (1989).

[15] F. Deák, A. Kiss, Z. Seres, G. Caskey, A. Galonsky, C.K. Gelbke, B. Remington, M.B. Tsang, and J.J. Kolata, Nucl. Phys. **A464**, 133 (1987).

[16] A. Kiss, F. Deák, Z. Seres, G. Caskey, A. Galonsky, L. Heilbronn, and B. Remington, Phys. Rev. C **38**, 170 (1988).

[17] Á. Horváth, F. Deák, Á. Kiss, Z. Seres, A. Galonsky, C.K. Gelbke, H. Hama, L. Heilbronn, D. Krofcheck, W.G. Lynch, D.W. Sackett, H.R. Schelin, M.B. Tsang, J. Kasagi, and T. Murakami, Phys. Rev. C **49**, 1012 (1994).

[18] F. Deák, A. Kiss, Z. Seres, G. Caskey, A. Galonsky, and B. Remington, Nucl. Instrum. Methods Phys. Res. Sect. A **258**, 67 (1987).

[19] D. Sackett, A. Galonsky, C.K. Gelbke, H. Hama, L. Heilbronn, D. Krofcheck, W. Lynch, H.R. Schelin, M.B. Tsang, X. Yang, F. Deák, Á. Horváth, Á. Kiss, Z. Seres, J. Kasagi, and T. Murakami, Phys. Rev. C **44**, 384 (1991).

[20] H.R. Schelin, A. Galonsky, C.K. Gelbke, H. Hama, L. Heilbronn, D. Krofcheck, W.G. Lynch, D. Sackett, M.B. Tsang, X. Yang, F. Deák, Á. Horváth, Á. Kiss, Z. Seres, J. Kasagi, and T. Murakami, Nuclear Science and Engineering **113**, 184 (1993).

[21] J.H. Heltsley, L. Brandon, A. Galonsky, L. Heilbronn, B.A. Remington, S. Langer, A. Vander Molen, J. Yurkon, and J. Kasagi, Nucl. Instrum. Methods Phys Res. Sect. A **263**, 441 (1988).

[22] R.A. Cecil, B.D. Anderson, and R. Madey, Nucl. Instrum. Methods **161**, 439 (1979).

[23] B.A. Remington, G. Caskey, A. Galonsky, C.K. Gelbke, A. Kiss, F. Deák, Z. Seres, J.J. Kolata, J. Hinnefeld, and J. Kasagi, Phys. Rev. C **34**, 1685 (1986).

[24] F. Ajzenberg-Selove, Nucl. Phys. **A490**, 1 (1988).

[25] F. Ajzenberg-Selove, Nucl. Phys. **A506**, 1 (1990).

[26] F. Ajzenberg-Selove, Nucl. Phys. **A523**, 1 (1991).

[27] G.J. Wozniak, H.L. Harney, K.H. Wilcox, and J. Cerny, Phys. Rev. Lett. **28**, 1278 (1972).

[28] H.M. Xu, W.G. Lynch, C.K. Gelbke, M.B. Tsang, D.J. Fields, M.R. Maier, D.J. Morrissey, T.K. Nayak, J. Pochodzalla, D.G. Sarantides, L.G. Sobotka, M.L. Halbert, and D.C. Hensley, Phys. Rev. C **40**, 186 (1989).

[29] J. Pochodzalla, C.K. Gelbke, W.G. Lynch, M. Maier, D. Ardouin, H. Delagrange, H. Double, C. Grégoire, A. Kyanowsky, W. Mittig, A. Péghaire, J. Péter, F. Saint-Laurent, B. Zwieglinski, G. Bizard, F. Lefébres, B. Tamain, J. Québert, and Y.P. Viyogi, Phys. Rev. C **35**, 1695 (1987).